Available online at www.sciencedirect.com
SCIENCE DIRECT®
Journal of Nuclear Materials 343 (2005) 227–235
journal of nuclear materials
www.elsevier.com/locate/jnucmat

Ductility recovery in structural materials for spallation targets by post-irradiation annealing

J. Chen *,[1], P. Jung, M. Rödig, H. Ullmaier, G.S. Bauer

Institut für Festkörperforschung und Projekt ESS, Forschungszentrum Jülich, D-52425 Jülich, Germany

Abstract

Low temperature irradiation embrittlement is one of the major criteria to determine the lifetime of spallation targets. Embrittlement is especially high at low service temperatures, e.g. 250 °C in liquid-mercury sources. It was the aim of the present study to investigate the effect of post-irradiation annealing on the mechanical properties of irradiated structural materials. The specimens used were obtained from spent target components of operating spallation facilities (Los Alamos Neutron Science Center, LANSCE, and the Spallation Neutron Source at Rutherford-Appleton Laboratory, ISIS). The investigated materials include a nickel-based alloy (IN718), an austenitic stainless steel (AISI 304L), a martensitic stainless steel (DIN 1.4926) and a refractory metal (Ta) which experienced 800 MeV proton irradiation to fluences of several 10^{25} p/m^2. The specimens were annealed from 300 °C to 700 °C for 1 to 10 h, respectively, and their mechanical property changes were subsequently investigated at room temperature and 250 °C by tensile testing and fracture surface analysis conducted by scanning electron microscopy (SEM). The results showed that the ductility recovered to a large degree in 304L and DIN 1.4926 materials while their strength remained almost unchanged. Especially for DIN 1.4926, the ductility recovery is remarkable already at 400 °C. Together with its favorable thermo-mechanical properties, this makes martensitic steel a candidate for structural materials of spallation targets.

1. Introduction

Structural materials issues are an important part of the R&D programs for spallation neutron sources of the MW class [1–3]. Some critical components such as beam windows and especially beam entrance windows of the mercury target container are subject to severe loads in terms of thermal stress, pressure waves and radiation dose, due to the high power and pulsed proton beam injection. These loads can cause mechanical failure, pitting, fatigue and radiation-induced embrittlement which determine the performance and lifetime of the components.

To select the optimum materials for the target stations of spallation neutron sources in the MW class, an extensive international materials R&D program focusing on radiation effects has been initiated in 1996, and a large number of papers in this topic have been published (see [4–7] for summaries). A wide class of materials is included in this program, for instance, nickel-based super alloys, austenitic stainless steels, ferritic/martensitic stainless steels, aluminum alloys and refractory metals. The published experimental results [4–7] have indicated that high energy proton irradiation

* Corresponding author. Tel.: +41 56 310 2280; fax: +41 56 310 4595.
E-mail address: jiachao.chen@psi.ch (J. Chen).
[1] Now with: Labor für Werkstoffverhalten, Paul Scherrer Institut, CH-5232 Villigen, Switzerland.

0022-3115/$ - see front matter © 2005 Elsevier B.V. All rights reserved.
doi:10.1016/j.jnucmat.2004.09.076

causes a substantial amount of hardening and a severe reduction in the ductility of metals and alloys, which are similar or even more critical compared to the case of reactor neutron irradiation. The most problematic radiation effect is embrittlement in the low irradiation temperature regime (<300 °C or saying below the recovery stage V) for all materials. Unfortunately this is the operating temperature regime for spallation neutron source with mercury targets. Because of critical embrittlement, it has been recommended that the SNS target, using 316LN (one of the best materials against irradiation embrittlement at low temperature) as a structural material, should be removed for examination after 5 dpa have been accumulated. This corresponds to only around 2 months of full power operation [2].

Microstructural studies have revealed that the dominant damage microstructures in the materials irradiated in a spallation environment at low temperatures are dense arrays of clusters of self-interstitial atoms (SIAs) and stacking fault tetrahedra (SFTs), referred to as 'black dots', and some interstitial Frank dislocation loops. Such defects formed in materials during irradiation act as obstacles for dislocation motion causing irradiation hardening, which can be accompanied by a loss of ability to work-harden (for a detailed discussion on the influence of irradiation-induced changes in the microstructure on the plastic deformation of different materials, see [8,9]). It is expected that post-irradiation annealing above the irradiation temperature can probably anneal the irradiation-induced defects and partially recover the ductility. This means that, besides materials selection, there is another possible way to extend the target lifetime, i.e. to develop an operation modus where radiation induced embrittlement can be partially annealed out.

Up to now, only a few experiments on copper and its alloys [10–13] have been performed in this connection. The data base for designing an optimum operation modus of the target station of spallation neutron sources is far away from being sufficient. In this paper we present preliminary tensile results on INCONEL 718, pure Tantalum, AISI 304L and DIN 1.4926 after post-irradiation annealing at temperatures in the range from 300 °C to 700 °C and annealing times from 1 to 10 h. The analysis of fracture surface observations is also given.

2. Experimental

The investigated spent targets and components are a LANSCE Water-Degrader, a LANSCE Beam-Window, a PSI Window irradiated in LANSCE and an ISIS target. The details of the materials, dimensions and operation conditions can be found in [4]. Only a brief description is given here. The Water-Degrader consisted of two concentric spherical shells made of IN 718 (outer shell) and AISI 304L (inner shell), respectively. It was irradiated with 760 MeV protons to a total charge of 5.3 Ah (= Ampere hours) at a maximum temperature of 250 °C. The LANSCE Beam-Window made of IN 718 is a hemispherical double-shell with cooling water flowing between the two shells and was used to separate the vacuum of the beam line and the target area. It was exposed to a total charge of approximately 3.4 Ah at around 400 °C. The water-cooled double-shell PSI-Window made of DIN 1.4926 was manufactured in the Paul Scherrer Institut, Switzerland and irradiated in LANSCE with 800 MeV protons to a total charge of 2.8 Ah at $\leqslant$230 °C. The ISIS target consisted of a target container with a window made of AISI 304L stainless steel and 23 water-cooled Ta plates which served as spallation material. The target was irradiated with a short-pulsed 800 MeV proton beam at temperatures lower than 200 °C. The total accumulated charge on the target was 1.7 Ah.

To specify the irradiation conditions, the profiles of the proton beam impinging on the spent target components were measured by γ-scans in the hot cells of FZ-Juelich. From the parameters of the distributions, the position of samples and the total charges, the following proton fluences of 2.3×10^{25} p/m^2 for AISI 304L, 6.4×10^{25} p/m^2 for IN 718, 2.2×10^{25} p/m^2 for DIN 1.4926 and 1.3×10^{25} p/m^2 for pure Ta were obtained. Taking displacement damage cross-sections of 2900b for 304L and IN 718 [14], 2600b for DIN 1.4926 [15] and 6650b for Ta [16], the corresponding displacement doses are 6.7, 20, 5.8 and 8.4 dpa for AISI 304L, IN 718, DIN 1.4926 and pure Ta, respectively. To determine the He- and H-concentrations in the materials, the production cross-sections of $\sigma_{He} = 0.58$b and $\sigma_H = 1.8$b for 304L and DIN 1.4926 [17], $\sigma_{He} = 0.52$b and $\sigma_H = 2.0$b for IN 718 [17] and $\sigma_{He} = 0.34$b for Ta [16] were used, and the resulting He- and H-concentrations are found to be 1300 and 4200 appm for 304L, 3330 and 13 000 appm for IN 718 and 1300 and 4000 appm for DIN 1.4926, respectively. Because of the unknown cross-section of H-production in Ta, only the He-concentration is calculated to be 540 appm. A summary of the irradiation conditions is given in Table 1. It should be noticed that the contribution of the fast neutrons to dpa and transmutation products is not included. At the position of the Water-Degrader, the LANSCE- and the PSI-Window, the flux of neutrons was very low and their contributions were estimated to be less than a few percent of the proton-induced values in the beam centre, while it is somewhat higher in the case of the ISIS target.

To prepare the miniaturized tensile specimens chosen for the present study, slabs of 15 mm length and 3 mm width were cut from the spent components and then polished down to 0.5 mm thickness. Finally dog-bone shaped tensile specimens with a gauge volume of

Table 1
Irradiation conditions

	LAMPF Beam-Window	ISIS target	LAMPF Water-Degrader	PSI Windows
	IN718	Ta	AISI 304L	DIN 1.4926
Proton energy (MeV)	800	800	760	760
Proton fluence (p/m^2)	6.4×10^{25}	1.3×10^{25}	2.3×10^{25}	2.2×10^{25}
Irrad. temp. (°C)	400	200	250	250
dpa	20	8.4	6.7	5.8
He (appm)	3300	440	1300	1300
H (appm)[a]	13000	–	4200	4000

[a] The values represent the hydrogen produced in materials. Because of the diffusional losses, the retained concentration of hydrogen should be lower.

$5\times1.5\times0.5$ mm^3 were machined. All specimen preparing work was done in the hot-cells at Forschungszentrum Juelich. Post-irradiation annealing was performed isothermally in vacuum of about 10^{-3} Pa at temperatures ranging from 300 °C to 700 °C for 1 and 10 h. Afterwards tensile test were conducted with a strain rate of about 10^{-3} at room temperature and 250 °C, using a 2 kN MTS tensile machine equipped with a video-extensometer. Subsequently, the fracture surfaces were observed by scanning electron microscopy, SEM (Hitachi S4100).

3. Results

3.1. INCONEL 718 alloy

Because of the estimated irradiation temperature of about 400 °C, the IN 718 specimens irradiated to 20 dpa were annealed at 500 °C and 700 °C, respectively, for 1 h. The specimens at both annealing temperatures were tensile tested at room temperature. Like the as-irradiated specimen [4], the tensile curves showed that the annealed specimens also failed without any plastic deformation, indicated by load drop just after the elastic portion of the curve. The changes in ultimate tensile strength and total elongation as a function of annealing temperature are shown in Fig. 1. The points on the ordinate refer to reference data. Assuming that no changes will occur if the specimen are annealed below the irradiation temperature, the as-irradiated data are plotted at both room and irradiation temperature in the figure. From a comparison between the reference and the as-irradiated data, a slight irradiation softening can be found. But the elongation drops to zero after irradiation to 20 dpa. The ultimate strength is slightly higher at an annealing temperature of 500 °C but shows a big jump to about 1700 MPa at 700 °C, even exceeding the reference value. Nevertheless the elongations are still zero after annealing. In the previous study [4], the IN 718 specimens showed fully intergranular fracture behaviour at 20 dpa. A similar fracture mode is anticipated because of the same failure behaviour in the tensile curves for all specimens. Therefore SEM investigations were not performed on post-irradiation annealed specimens.

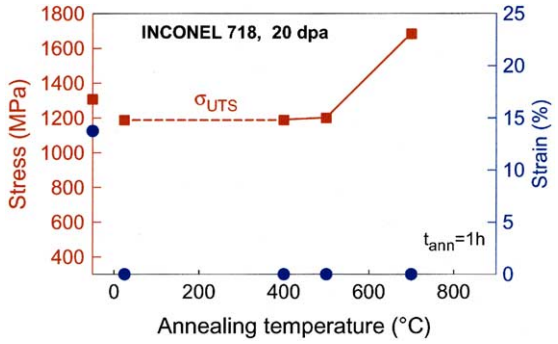

Fig. 1. Ultimate tensile strengths (■) and total elongations (●) as a function of post-irradiation annealing temperature for INCONEL 718 alloy. The points on the ordinate refer to reference data. The solid and dashed lines serve as a guide to the eye.

3.2. Tantalum

Fig. 2 presents the tensile curves for pure Ta before irradiation, as-irradiated and after post-irradiation annealing, tested at room temperature. The tensile results showed irradiation hardening and a somewhat reduced elongation. However, the tensile stress after post-irradiation annealing is increased instead of its expected decrease and the tensile elongation is decreased instead of the expected increase for post-irradiation annealed specimen. We should mention that the specimen annealed at 700 °C for 1 h broke into pieces during handling with the manipulator in the hot-cells, suggesting that the Ta suffered enhanced hardening and embrittlement during post-irradiation annealing.

3.3. AISI 304L austenitic stainless steel

The stress–strain curves for the un-irradiated, as-irradiated and post-irradiation annealed AISI 304L

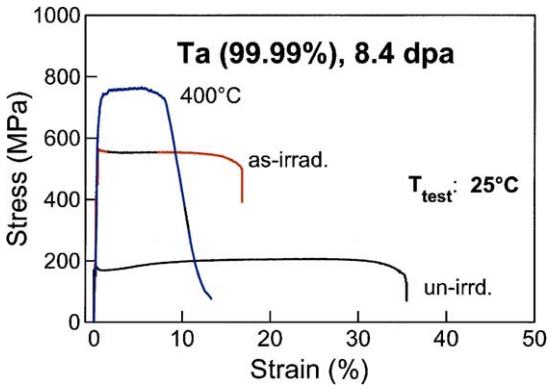

Fig. 2. Stress–strain curves of pure tantalum specimens tested at a strain rate of 10^{-3}/s at RT.

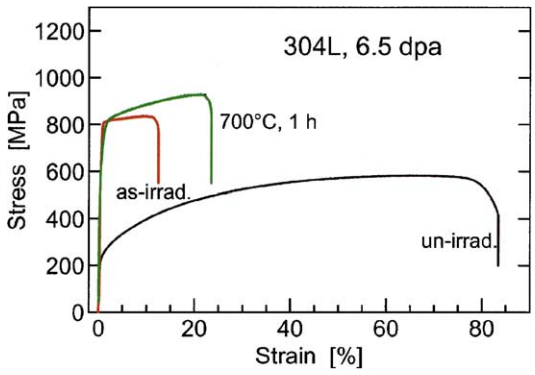

Fig. 3. Stress–strain curves of AISI 304L specimens tested at a strain rate of 10^{-3}/s at RT.

specimens, tested at room temperature, are given in Fig. 3. The tensile curve of the irradiated specimen shows the normal trend of an irradiation-induced increase in strength and decrease in ductility. Note that the flat top of the curve indicates an almost complete loss of engineering work hardening ability. On the other hand, the behavior after post-irradiation annealing is substantially different. Though the yield strength is similar to the as-irradiated one, the uniform elongation is almost doubled. The most interesting feature is that the post-irradiation annealed specimen exhibits a substantial amount of work hardening and the tensile strength becomes even higher than in the irradiated case.

SEM micrographs of the fracture surfaces are given in Fig. 4 for the un-irradiated, as-irradiated and post-irradiation annealed specimens. The fracture surface of the un-irradiated specimen is shown in Fig. 4(a) which illustrates a typical dimpled transgranular ductile fracture mode. For the irradiated specimen, Fig. 4(b), the fracture mode changes to partial (60%) intergranular brittle failure. After post-irradiation annealing treatment, the fracture mode is completely the same as the un-irradiated one, see Fig. 4(c). The reduction-in-area is 73%, 25%, and 63% for un-irradiated, as-irradiated and post-irradiation annealed specimens, respectively.

3.4. DIN1.4926 martensitic stainless steel

Due to its favorable thermo-mechanical properties, martensitic stainless steels are interesting materials for MW class spallation neutron sources. But this type of materials suffers a severe decrease in the uniform elongation already at a dose level of about 1 dpa [4,6,18] at low

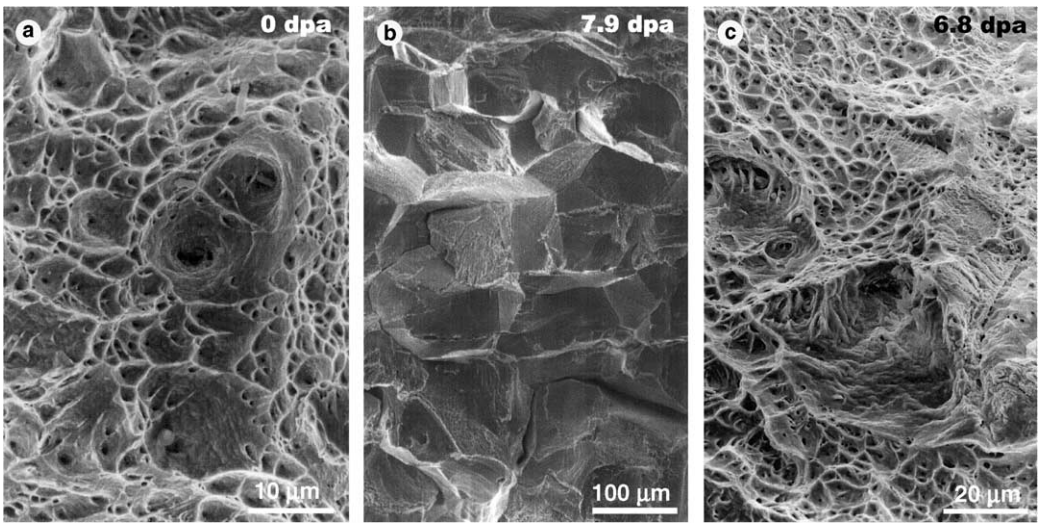

Fig. 4. Scanning electron micrographs show the fracture morphology of AISI 304L after tensile tests at a strain rate of 10^{-3}/s at RT, (a) un-irradiated, (b) as-irradiated, (c) post-irradiation annealed.

irradiation temperatures (<300 °C). According to its application interests, the post-irradiation annealing is performed at temperature of 300 °C, 350 °C, 400 °C and 700 °C, respectively, for 1 h and tensile tested at room temperature. Additionally, two specimens have been annealed at 350 °C for 10 h and tested at RT and 250 °C, respectively.

The stress–strain curves for DIN 1.4926 irradiated to 5.8 dpa and annealed at different temperatures are given in Fig. 5, showing the effects of annealing temperature. For comparison, the stress–strain curve for the un-irradiated specimen is also included. Clearly, compared to the un-irradiated case, the yield stress of as-irradiated specimen is increased by a factor of 2.4. The material loses its work hardening capability and begins necking after small strains (<1%). The most interesting feature of the results presented in Fig. 5 is that by increasing the annealing temperature, the yield strengths decrease only slightly, but the dropping portion of the curves are bending up gradually to become comparable to the un-irradiated material at 700 °C. This is connected to a large amount of recovery in uniform elongation. The yield stresses, ultimate tensile strengths, uniform elongations and total elongations as a function of annealing temperature are summarized in Fig. 6. The points on the ordinate refer to un-irradiated material. Similar to Fig. 1, as-irradiated data are plotted at both RT and irradiation temperature. Note that the tensile stresses remain almost constant during annealing, but the elongations recover remarkably until being almost complete at 700 °C.

The effects of annealing time and test temperature are illustrated in Fig. 7(a) and (b), respectively. The tensile properties of the specimens annealed at 350 °C for 1 and 10 h are rather similar, indicating a minor influence of annealing time. The specimens tested at 250 °C show similar recovery of uniform elongation whereas the yield stress is reduced more strongly in comparison with specimens tested at RT.

Despite severe reduction of uniform elongation, the failure mode of DIN 1.4926 was found to be ductile for all cases, i.e. un-irradiated, as-irradiated and post-irradiation annealed materials, tested at RT and 250 °C. This is significantly different from classic

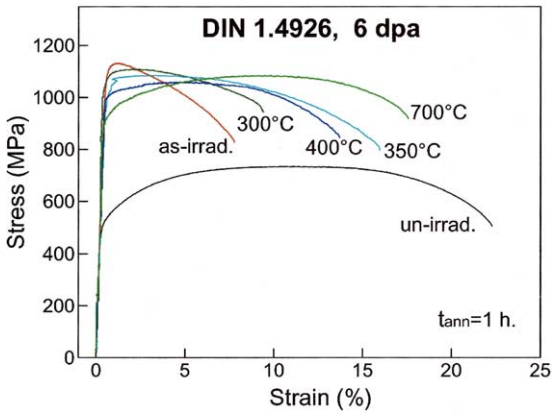

Fig. 5. Stress–strain curves of martensitic stainless steel DIN 1.4926 after post-irradiation annealing at various temperatures. For comparison, un-irradiated and as-irradiated specimens are also included. The tensile tests were performed at a strain rate of 10^{-3}/s.

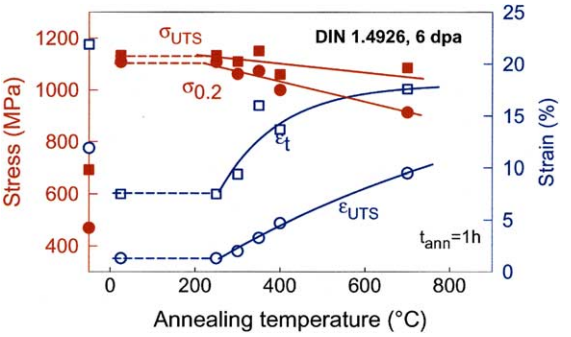

Fig. 6. Yield stresses (0.2% offset), ultimate tensile strengths, uniform elongations and total elongations are plotted as a function of post-irradiation annealing temperature. Filled and empty symbols indicate stress and strain, respectively. The points on the ordinate refer to reference data. The lines in the figure serve as a guide to the eye.

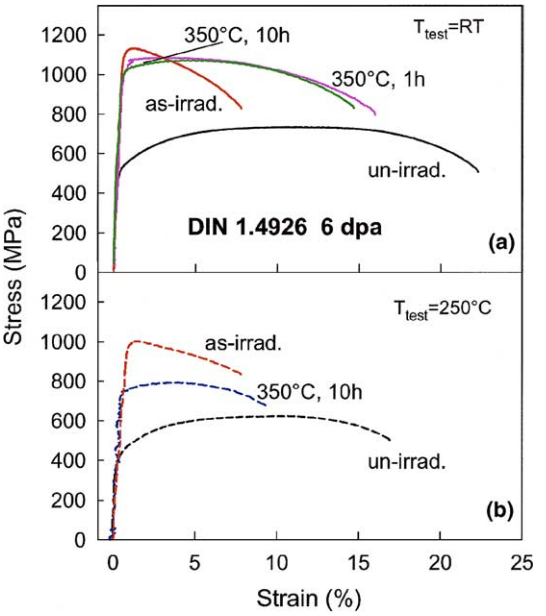

Fig. 7. Stress–strain curves of martensitic stainless steel DIN 1.4926 un-irradiated, as-irradiated and post-irradiation annealed, tested at RT (a) and at 250 °C (b).

embrittlement. One example of SEM investigation is given in Fig. 8, showing a typical transgranular ductile failure. From SEM micrographs, the reduction in area (RA) after tensile testing was measured and is plotted in Fig. 9 as a function of annealing temperature. The

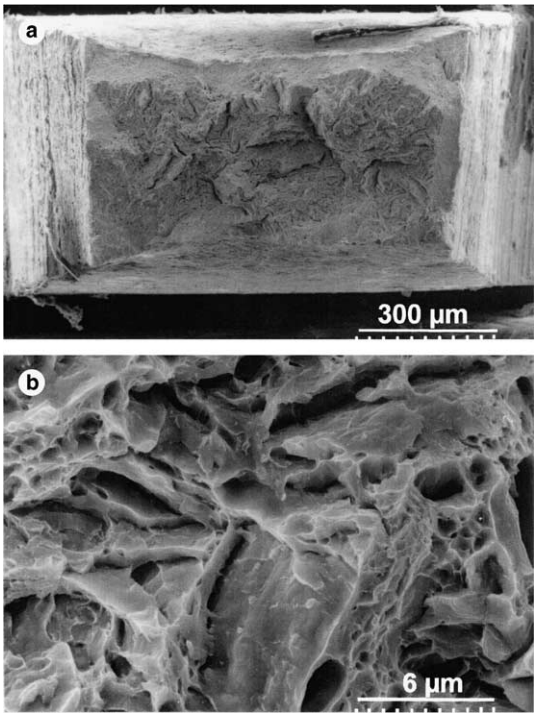

Fig. 8. Scanning electron micrographs of the fracture morphology of 6 dpa martensitic stainless steel DIN 1.4926 after post-irradiation annealing at 350 °C for 10 h (a). (b) is shows an enlarged part of (a).

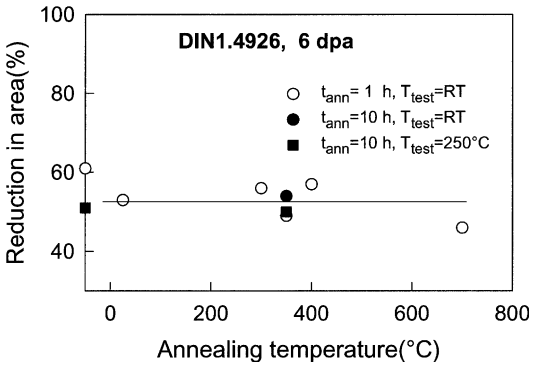

Fig. 9. Reduction in area of martensitic stainless steel DIN 1.4926 as a function of the post-irradiation annealing temperature. The data from different annealing times and test temperatures are also included. The points on the ordinate refer to reference data. The line in the figure serves as a guide to the eye.

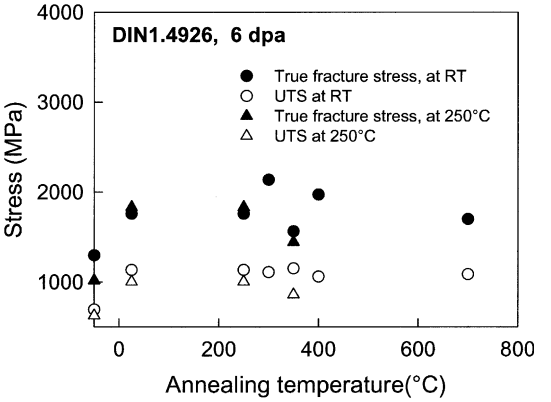

Fig. 10. Comparison of true fracture stress and ultimate tensile stress as a function of the post-irradiation annealing temperature. The filled and open symbols indicate true fracture stress and ultimate tensile strength, respectively. The circles and triangles are for specimens annealed for 1 h and tested at RT, and annealed for 10 h and tested at 250 °C, respectively. The points on the ordinate refer to reference data.

data from specimens annealed at 350 °C for 10 h and tested at RT and 250 °C are also included. It should be emphasized that the RA of the material was more than 50% for all conditions. The true fracture stress can be calculated from the load in failure determined from the tensile curves and the corresponding actual cross-section area measured by SEM. The results for DIN 1.4926 as a function of annealing temperature are illustrated in Fig. 10, which demonstrates again the large local plastic deformation occurring in the necking region.

4. Discussion and conclusions

The results presented above reveal a quite different annealing behaviour of the tensile properties for the different materials. To understand those differences, it is necessary to follow the changes in the microstructural development, because the mechanical property changes in irradiated materials are the direct result of the evolution of the damage microstructure. Irradiation hardening has been treated with a dispersed barrier hardening (DBH) model (see [19] for a review), where the increase in yield stress is proportional to the square root of the product of the size and density of obstacles such as dislocation loops, SFTs, cavities and other features formed during irradiation. Recently, to predict the yield drop and subsequent flow localization observed in materials, Singh et al. [20] proposed a cascade-induced source hardening (CISH) model. The main idea is that during irradiation under cascade damage conditions, the grown-in dislocations become decorated by clusters of self-interstitial atoms (SIAs). The decoration effectively

pins the dislocations and prevents them from acting as dislocation sources until the applied stress reaches a high level to free the dislocations from the atmosphere of clusters and loops decorating them. The following discussion will partly be based on this concept.

In the present experiments INCONEL 718 revealed an unusual annealing of the hardening and embrittlement. A possible explanation is as follows [21]. In original condition the strengthening precipitates such as γ' and γ'' act as hard particle obstacles causing Orowan hardening. During irradiation, they become disordered at low doses (<0.6 dpa) [21] and the solutes from the former precipitates are redistributed gradually in the matrix with the increase of the doses. The tensile test exhibited slight softening at high dose. However, according to a previous study, the precipitates restructured again at an annealing temperature of 500 °C [22]. Furthermore helium bubbles formed at 700 °C [22] and the dislocation density observed in TEM was still very high. This can qualitatively explain the unusual annealing behavior of INCONEL 718. But it is still unclear why the material becomes totally brittle.

The observed annealing behavior of hardening and embrittlement in pure Ta was probably reflecting artifacts of the annealing conditions. The mechanical properties of refractory metals like Ta and W are very sensitive to interstitial impurities. Actually, a drastic embrittlement has already been observed at very low neutron doses on 'technical' Ta [23] which contains high concentrations of C, N and O. Therefore the most likely reason for the reported unusual 'annealing' behaviour is interstitial impurities pick-up during our annealing in poor vacuum (around 10^{-3} Pa). To fully understand the changes appearing in INCONEL 718 and pure Ta is very difficult due to synergy effects between solutes or impurity atoms and irradiation-induced defects.

In contrast to those findings, our experiments showed annealing-improved ductility on AISI 304L without reduction of yield stress. TEM investigation revealed that the dense population of nano-size defect clusters ('black dots') had disappeared and network dislocations were formed (see Fig. 11) after post-irradiation annealing at 700 °C for 1 h. The network dislocations became the dominant obstacles which contribute to maintaining the high strength of the material. Additionally, the network dislocations probably impede the development of channel bands during tensile testing. Such channel bands are believed to influence work softening and plastic instability. In spite of the very high yield stress (800 MPa) in the specimen after post-irradiation annealing, the material can further work harden during the tensile test. The dislocations alone as obstacles cannot account for such a high strength because the ultimate tensile strength is already twice as high as for un-irradiated specimens. One possibility is that defect clusters, seen as black dots, and produced during plastic deformation [24] will

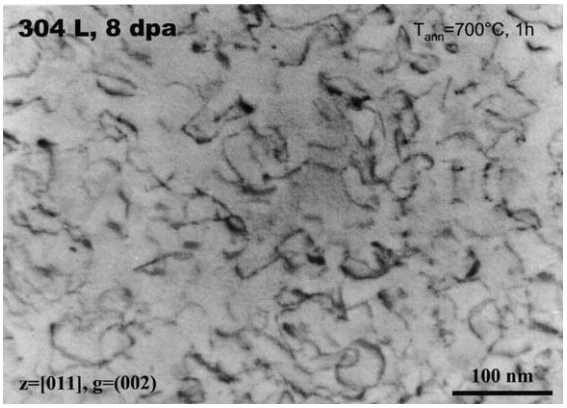

Fig. 11. Microstructural features of AISI 304L irradiated to 8 dpa and subsequently annealed at 700 °C for 1 h, showing the network dislocations.

contribute to further hardening. If this is true, the post-irradiation annealing treatment should be an intriguing method to cure materials in a low temperature irradiation environment. Choosing suitable annealing parameters, where nano-size defect clusters are annihilated and network dislocation are formed, the materials will not only maintain high strength but also have high ductility. Dislocations are relatively weak obstacles in materials and will not cause severe embrittlement. On the other hand, according to the superposition law in the DBH model [19], the total change in stress is simply the sum of the contributions of long-range type and short-range type barriers. It is, however, the square root of the sum of the squared changes induced by barriers of the same type. Network dislocations are usually treated as long-range obstacles whereas the small clusters and remainders of the irradiation-induced defects are considered as short-range. Here we give an example. For instance, one can assume that irradiation-induced defects alone could produce a typical change of 500 MPa in strength and the small clusters induced by plastic deformation alone could cause a further change of 50 MPa in strength during subsequent tensile testing. Then a total change of $\sqrt{500^2 + 50^2} = 502.5$ MPa can be expected. In this case, the work hardening due to small clusters can be neglected. But if small defects produced by irradiation are annealed out, work hardening due to small clusters can contribute 50 MPa to the total change in strength and the material will indeed exhibit work hardening. Of course, further investigations are needed to prove this conjecture.

In principle, the above consideration is also valid for martensitic steel. Here one fact should be mentioned. Though the irradiation hardening can reach up about 600 MPa in martensitic steels, the measured density of visible defect clusters was one order of magnitude lower than in austenitic steels [18,25]. Does this suggest that

clusters formed in martensitic steels are smaller and below the TEM' resolution? It would make an analysis more difficult. Anyhow, from an engineering application point of view, very interesting and beneficial changes were found on DIN 1.4926. The post-irradiation annealing manifested an annealing-improved ductility of DIN 1.4926. Especially, it eliminated the problem of plastic instability and restored enough uniform elongation to make the martensitic stainless steel DIN 1.4926 useful again. Because the stress loads in a mercury container made of martensitic stainless steels will be much lower than in one made of austenitic stainless steels since the former have higher thermal conductivity and less thermal expansion (see [4] for details), martensitic stainless steel will be promising candidates if their embrittlement problem can be solved. The present results demonstrate the potential to employ post-irradiation annealing treatments for extending the lifetime of these materials. Of course, the present study is not sufficient to propose an optimized operation mode. A recent experimental study on the effects of irradiation-annealing-irradiation cycles for copper and its alloy [13], indicate rather optimistic prospects. However, considering the very low doses and the different material explored in [13], it should be experimentally verified that the conclusions are valid also in a high-dose spallation source environment.

Finally it should be mentioned that our results on the recovery of the tensile properties of martensitic steels have been confirmed by measurements on specimens implanted by helium (up to 2500 appm He and 0.4 dpa) [26].

Based on the present results and their discussion, the following summary and conclusion can be drawn.

- Annealing results showed an unusual effect of annealing hardening in INCONEL 718. The possible mechanism is restructuring of precipitates and bubble formation.
- The observed of hardening and embrittlement due to annealing of irradiated pure Ta can be assigned to artifacts of the annealing conditions.
- During post-irradiation annealing (700 °C), AISI 304L showed (1) partial recovery of ductility, (2) almost complete retention of strength, (3) partial recovery of work hardening ability and (4) recovery of the fracture mode (from partial intergranular to complete transgranular ductile).
- During post-irradiation annealing ($\geqslant$350 °C), DIN 1.4926 revealed (1) almost complete recovery of ductility, (2) almost complete retention of strength, (3) partial recovery of work hardening ability and (4) almost no effects on fracture behavior.
- The annealing effects of AISI 304L and DIN 1.4926 can be qualitatively explained in terms of DBH and CISH models.

We suggest that the possibility to cure the irradiation induced embrittlement by annealing at relatively modest temperatures, together with their favorable thermo-mechanical properties, should lead to a re-consideration of martensitic steels as candidates for structural materials in spallation targets, especially for sources in the MW power range.

Acknowledgments

The authors would like to thank Dr S.A. Maloy, Dr W.F. Sommer and Dr T. Broome for supply of the spent components. Thanks also to G. Behrens, Mr T. Flossdorf and Mr W. Kalf for their technical assistance to prepare the specimens and perform the tensile tests in the hot-cells.

References

[1] G.S. Bauer, H. Ullmaier, J. Nucl. Mater. 318 (2003) 26.
[2] L.K. Mansur, J. Nucl. Mater. 318 (2003) 14.
[3] K. Kikuchi, T. Sasa, S. Ishikura, K. Mukugi, T. Kai, N. Ouchi, I. Ioka, J. Nucl. Mater. 296 (2001) 34.
[4] J. Chen, G.S. Bauer, T. Broome, F. Carsughi, Y. Dai, S.A. Maloy, M. Roedig, W.F. Sommer, H. Ullmaier, J. Nucl. Mater. 318 (2003) 56.
[5] Y. Dai, G.S. Bauer, J. Nucl. Mater. 296 (2001) 43.
[6] S.A. Maloy, M.R. James, G. Willcutt, W.F. Sommer, M. Sokolov, L.L. Snead, M.L. Hamilton, F. Garner, J. Nucl. Mater. 296 (2001) 119.
[7] K. Farrell, T.S. Byun, J. Nucl. Mater. 296 (2001) 129.
[8] T.S. Byun, K. Farrell, Acta Mater. 52 (2004) 1597.
[9] G.R. Odette, M.Y. He, E.G. Donahue, P. Spätig, T. Yamamoto, J. Nucl. Mater. 307–311 (2002) 171.
[10] B.N. Singh, D.J. Edwards, P. Toft, J. Nucl. Mater. 299 (2001) 205.
[11] S.A. Fabritsiev, A.S. Pokrovsky, J. Nucl. Mater. 307 (2002) 431.
[12] D.J. Edwards, B.N. Singh, Q. Xu, P. Toft, J. Nucl. Mater. 307 (2002) 439.
[13] S.A. Fabritsiev, A.S. Pokrovsky, S.E. Ostrovsky, J. Nucl. Mater. 324 (2004) 23.
[14] S.L. Green, J. Nucl. Mater. 126 (1984) 30.
[15] M. Wechsler, M.H. Barnett, D.J. Dudziak, L.K. Mansur, L.A. Charlton, J.M. Narnes, J.O. Johnson, in: Proceedings of the Symposium on Materials for spallation Neutron Sources, Orlando, 10–12 February 1997.
[16] D. Filges, C. Mayr, R.D. Neef, H. Schaal, A. Tietz, J. Wimmer, ESS report No. 96-45-T (1996).
[17] F.A. Garner, B.M. Oliver, L.R. Greenwood, M.R. James, P.D. Ferguson, S.A. Maloy, W.F. Sommer, J. Nucl. Mater. 296 (2001) 66.
[18] Y. Dai, S.A. Maloy, G.S. Bauer, W.F. Sommer, J. Nucl. Mater. 283–287 (2000) 513.
[19] G.E. Lucas, J. Nucl. Mater. 206 (1993) 287.
[20] B.N. Singh, A.J.E. Foreman, H. Trinkaus, J. Nucl. Mater. 249 (1997) 103.

[21] B.H. Sencer, G.M. Bond, F.A. Garner, M.L. Hamilton, S.A. Maloy, W.F. Sommer, J. Nucl. Mater. 296 (2001) 145.
[22] J. Chen, S. Romanzetti, W.F. Sommer, H. Ullmaier, J. Nucl. Mater. 304 (2002) 1.
[23] F.W. Wiffen, in: R.J. Arsenault (Ed.), Proc. 1973 International Confernece on Defect Clusters in B.C.C. Metals and Their Alloys, Washington, DC, 1973, p. 176.
[24] Yong Dai, PH.D. Thesis (No. 1388), University of Lausanne, 1995, p. 80.
[25] Y. Dai, X. Jia, J.C. Chen, W.F. Sommer, M. Victoria, G.S. Bauer, J. Nucl. Mater. 296 (2001) 174.
[26] P. Jung, J. Chen, K. Klein, Proceedings of the Seventh International Workshop on Spallation Materials Technology, Thun, Switzerland, May 29–June 3, 2005, accepted for publication.